Submitted Manuscript: Confidential

N-Aryl Linked Spirocyclic Polymers for Membrane Separations of Complex Hydrocarbon Mixtures

Authors: Kirstie A. Thompson,[†1] Ronita Mathias,[†2] Daeok Kim,[3] Jihoon Kim,[3] Neel Rangnekar,[4] J.R. Johnson,[4] Scott J. Hoy, [5] Irene Bechis,[6] Andrew Tarzia,[6] Kim E. Jelfs,[6] Benjamin A. McCool,[4] Andrew G. Livingston,[3,7] Ryan P. Lively,*[2] M.G. Finn*[1]

Affiliations:

[1]School of Chemistry & Biochemistry, Georgia Institute of Technology, Atlanta, GA 30332, USA

[2]School of Chemical & Biomolecular Engineering, Georgia Institute of Technology, Atlanta, GA 30332, USA

[3]Department of Chemical Engineering, Imperial College London, London SW7 2AZ, UK

[4]Corporate Strategic Research, ExxonMobil Research and Engineering, Annandale, NJ 08801, USA

[5]Analytical Sciences Laboratory, ExxonMobil Research and Engineering, Annandale, NJ 08801, USA

[6]Department of Chemistry, Imperial College London, London W12 0BZ, UK

[7]School of Engineering and Materials Science, Queen Mary University of London, London E1 4NS, UK

D.K. present address: Environment & Safety Research Center, Samsung Electronics, 1, Samsungjeonja-ro, Hwaseong-si, Gyeonggi-do, South Korea

*Correspondence to: ryan.lively@chbe.gatech.edu; mgfinn@gatech.edu

† equal contributions

Abstract: The fractionation of crude oil mixtures via distillation is a large-scale, energy-intensive process. Membrane materials can avoid phase changes in such mixtures and thereby reduce the energy intensity of these thermal separations. With this application in mind, we created spirocyclic polymers with N-aryl bonds that demonstrated non-interconnected microporosity in the absence of ladder linkages. The resulting glassy polymer membranes demonstrated nonthermal membrane fractionation of light crude oil through a combination of class- and size-based "sorting" of molecules. We observed an enrichment of molecules lighter than 170 Da corresponding to a carbon number of 12 or boiling point less than 200°C in the permeate. Such scalable, selective membranes offer potential for the hybridization of energy-efficient technology with conventional processes like distillation.

One Sentence Summary: Spirocyclic polymers enable nonthermal separation of crude oil components.

Main Text:

Each day approximately 100 million barrels of crude oil are fractionated in refineries around the globe, primarily by thermal distillation. Though distillation has the potential for high recoveries of molecules in discrete boiling point ranges, it is energy-intensive, requiring more than 1100 terawatt-hours per year — nearly 1% of global energy use (*1*). Distillation energy and carbon efficiency could be improved if it were paired with low energy membrane-based separations that fractionate complex mixtures containing thousands of compounds into smaller groups of molecules. Membrane separations based on molecular differences in size, shape, and membrane-penetrant interactions have the potential for a ten-fold increase in energy efficiency over thermal processes (*2*). Seawater reverse osmosis systems that currently process greater liquid flows than the largest refineries highlight the potential for membrane technology to match the scales required by the hydrocarbon processing industry. While membrane technologies are established for certain aqueous and gas separations, they have not been developed for the fractionation of organic solvent mixtures, due to the relative scarcity of effective materials that are easily processable, inexpensive, and stable (*3*). Polymeric membrane materials provide the best combination of these three metrics, but to date have not been sufficiently effective for separations of small liquid organic molecules.

Polymers of intrinsic microporosity (PIMs) with their contorted ladder-like structures have high guest permeability and have therefore been widely studied for gas separations and to some extent for organic solvent separations (*4-6*). For the prototypical polymer **PIM-1**, there is a significant disparity between the apparent pore size distributions in the "dry" and organic solvent "wet" states. Cryogenic physisorption experiments in solid **PIM-1** suggest an average pore size between 3.5 and 5.0 Å (*7*). In contrast, molecular weight cut-off measurements of styrene oligomers in toluene by **PIM-1** membranes was reported (and was confirmed here) to be greater than 600 g-mol^{-1} (*8*), which corresponds to a pore size of 14 Å in a rigid membrane material such as a ceramic (*9*). This discrepancy derives from motion-enabled zones of activation in the semi-rigid polymer network that undergo swelling and plasticization in organic solvents (*5*). A PIM-like polymer that does not exhibit these phenomena should enable separations of small molecules in the organic solvent reverse osmosis (< 200 g-mol^{-1}) and "tight" organic solvent nanofiltration (200-300 g-mol^{-1}) regimes. While post-polymerization modifications can tune the properties of **PIM-1**-like materials (*10*), structures capable of performing difficult separations without post-polymerization or post-fabrication modification would provide more chances to create solutions to these impactful large-scale challenges.

We took note of previous gas separation work by McKeown and colleagues in which a spirobifluorene monomer was found to frustrate chain packing and rigidify ladder-type polymer structures beyond equivalent materials made using a spirobisindane monomer (*6*), resulting in higher polymer free volume and permeability relative to **PIM-1**. Moreover, swelling and plasticization were reduced, resulting in no apparent loss of separation selectivity compared to **PIM-1**. We therefore employed a similar spirobifluorene building block, but realized that this modification alone would likely be unable to address the challenge posed by swelling in organic solvent separation compared to gas-phase separations. Thus, we sought to enhance packing efficiency within certain segments of the backbone by using a modestly flexible linkage, choosing the aryl-N-aryl connection.

This design allowed the use of catalytic C-N bond formation as the polymerization process, rather than the nucleophilic aromatic substitution reaction that gives rise to the dibenzodioxin linkage of **PIM-1**. The palladium-catalyzed Buchwald-Hartwig amination reaction is a robust method for the coupling of aryl halides and amines that has been used extensively in medicinal, materials, and natural products chemistry (*11*); its application to polymer synthesis has been more limited. We chose a single spirobifluorene dibromide (**1**, Fig. 1 and Fig. S1) as the A-A monomer and a range of commercially available aromatic diamines as the B-B component (compounds **I-IV** in Fig. 1). Polymerization using the XantPhos Pd G4 palladacycle catalyst (*12*) was optimized (Table S1) with respect to temperature and concentration, providing the **s**piro**b**ifluorene **a**ryl **d**iamine (SBAD) series (Fig. 1).

All SBAD polymers were readily soluble in volatile solvents (THF, chloroform, CH_2Cl_2, Fig. S2) and were easily cast into films. GPC analysis revealed a component of high apparent molecular weight, thought to correspond to a small amount of branched material derived from a second N-H insertion event at one or more amine sites along the polymer chain (Fig. S3). Even a small amount of branching at secondary amine centers can dramatically inflate observed weight-average molecular weights and dispersities (*13*). The SBAD polymers demonstrated high thermal stabilities, with no observable glass transition temperatures (Figs. S4-S5), as has often been reported for PIM systems (*14*). These materials also exhibited low uptakes of N_2 at 77K (Fig. S6A) but had only moderately lower CO_2 sorption than **PIM-1** at 273K (Fig. 1B), suggesting the existence of isolated microporous free volume elements.

To further probe the pore structure of these materials, computational models for the polymers in the dry state were generated using the polymerization algorithm Polymatic (*15*). Three models were generated for each system to sample different structural arrangements and ensure the models were representative of the bulk material. The properties of the models were then characterized (Figs. S7-S8 and Table S2) (*16*). **PIM-1** and the SBAD series models showed similar predicted densities (Table S3) but significant differences in polymer voids, as seen in Fig. 1A, Fig. S9 and Table S3. The diameter of the largest probe that can pass through an interconnected pore network in the **PIM-1** models is 3.2 ± 0.3 Å, whereas the equivalent value for the SBAD series is 2.3 ± 0.1 Å. Only a small amount of flexible breathing motions or polymer swelling would be required for nitrogen (diameter 3.64 Å (*16*)) to diffuse through **PIM-1**, but much larger dilations would be required with the SBAD series (Fig. S10-11). This is consistent with the observed nitrogen physisorption isotherms (Fig. S6) showing high uptakes for **PIM-1** compared to the SBAD series at low relative pressures, which is the range that is typically used to calculate micropore distributions. By defining "interconnected pores" as those that are accessible by N_2 at 77K within a reasonable timeframe (2 days), it is apparent that "interconnected microporosity" is a characteristic feature of **PIM-1** that is suppressed in the SBAD polymers. This effect is likely due to the absence of the dibenzodioxin linkage and ladder-like morphology of **PIM-1** (Figs. S12-S13), replaced in the SBAD series with more flexible single-bond C-N linkages, allowing for the formation of π-π stacking interactions between and within chains (Fig. S14) and more efficient chain packing.

The computational work also suggests the existence of narrow distributions of ultra-micropores between 2-8 Å for **SBAD-1** and **-3** and 2-10 Å for **SBAD-2** and **-4**, whereas **PIM-1** has an apparently broader distribution between 2-12 Å (Figs. S15-S16). Even tighter distributions of ultra-micropores are seen in traditional glassy polymers (*17*), but the pore sizes are often too small for meaningful organic solvent separations. Thus, the presence of

intermediate non-interconnected pores exhibited by the SBAD materials could offer significant penetrant-penetrant differentiation of small-molecule organic solvents at reasonable fluxes if diffusion from one pore to the next were reasonably fast. In the "wet" state, separating small organic molecules requires that the membrane material exhibit resistance to significant solvent-induced swelling (e.g., Torlon®, a highly solvent-stable polyamide-imide, Fig. 1C). Solvent-induced dilation experiments showed that SBAD-1 experienced substantially less mass change than **PIM-1** at unit activity of toluene (Fig. 1C), suggesting that the SBAD materials retain their narrow distribution of ultramicropores even when exposed to solvents.
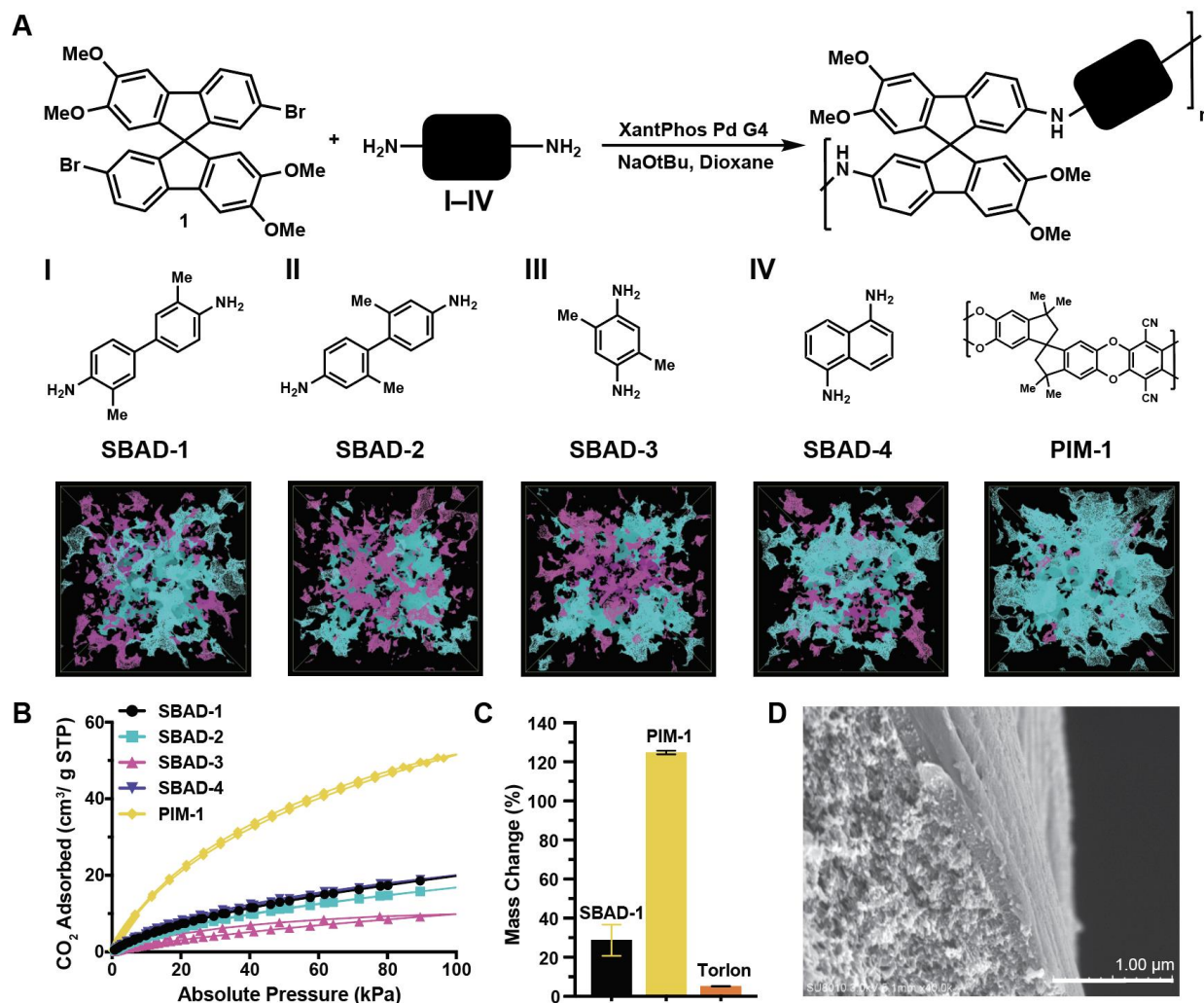
Fig. 1. Modular reaction scheme, computational simulation of porosity, powder physisorption, liquid sorption, and spectroscopic characterization. (A) Polymerization of 7,7'-dibromo-2,2',3,3'-tetramethoxy-9,9'-spirobifluorene, **1**, with diamines I–IV giving the SBAD class of materials: **SBAD-1–4**. Below the diamine structures are representative results of computational modeling of the pore surfaces for the SBAD series compared to **PIM-1** applying a 2.2 Å probe diameter, the largest probe that can pass through the SBAD materials; teal = accessible (interconnected) surface area, magenta = non-accessible surface area. (B) CO_2 uptake (at 273 K) by SBAD polymers compared to **PIM-1**. (C) Uptake of liquid toluene by dense films of **SBAD-1**,

PIM-1 and **Torlon®** (*22*), (*N*=2) 22°C, 1 atm. Data are the mean of 2 films +/- the range. (D) SEM image of **SBAD-1** thin-film composite showing an approximate barrier-layer thickness of 200 nm.

Mechanically robust thin film composite membranes were fabricated on crosslinked polyetherimide supports with no observable interlayer delamination (Fig. 1D and Fig. S17). The molecular separation performance of these materials was surveyed with binary mixture separations of 1,3,5-triisopropylbenzene (TIPB) in toluene (Fig. 2A). TIPB serves as a surrogate solute molecule for organic solvent separations, with a molecular weight (204.35 Da) at the lower end of the typical nanofiltration range (200-1000 g-mol^{-1}) in which PIMs have often been tested (*9*). Membrane performance was evaluated via cross flow filtration (Fig. S18) after more than 48 hours of continuous permeation of the mixture.

As shown in Fig. 2A, all of our polymers exhibited significantly greater rejections at steady-state than **PIM-1**, with permeances in the range of 0.1-0.7 L-m^{-2}-h^{-1}-bar^{-1}. **SBAD-1** showed the highest TIPB rejection of 80% throughout the duration of the experiment and **SBAD-3** was the least effective, despite having similar predicted micropore size distributions as the other materials. The most relevant structural difference appeared to be the larger biphenyl bridge structure used in **SBAD-1**, **2**, and **4** vs. the smaller phenyl bridge in **SBAD-3**. The improvement in TIPB rejection with the larger bridge suggests that aromatic chain-chain interactions, more available with biphenyl linkages (Fig. S14), are advantageous. The rejection properties of **SBAD-2** and **SBAD-4** increased over 48 hours, reaching steady-state values only slightly lower than **SBAD-1** (Fig. S19). Such time-dependent behavior is consistent with solvent-induced polymer relaxation towards a less swollen state (*18*). Only a handful of commercial organic solvent nanofiltration membranes and other polymeric membranes with complex fabrication procedures are capable of high rejections of ~200 g-mol^{-1} solutes and have toluene permeances in the same range (*9*). As **SBAD-1** demonstrated the highest rejections, it was chosen for scale-up and further evaluation with more complex mixtures.

SBAD-1 and **PIM-1** were compared in a standardized measurement of molecular weight cut-offs using oligostyrene markers in toluene. **SBAD-1** was significantly better than **PIM-1** in the separation of small solutes (molecular weight cut-off of 335 vs. 1220 g-mol^{-1}, respectively), albeit at a much lower permeance (0.2 L-m^{-2}-h^{-1}-bar^{-1} vs. 3.49 L-m^{-2}-h^{-1}-bar^{-1}). The molecular weight cut-off of **PIM-1** increased over the course of 3 days while that of **SBAD-1** remained constant (Fig. S20).

The separation performance of **SBAD-1** using a group of non-polar hydrocarbon molecules in the organic solvent reverse osmosis and nanofiltration ranges that are representative of hydrocarbons found in light crude oils is shown in Fig. 2C. A hydrocarbon molecular weight cut-off of approximately 253 g-mol^{-1} (Fig. S21) was calculated. Below 150 g-mol^{-1}, greater aromaticity (ratio of aromatic carbons to aliphatic carbons) of the solute was found to diminish rejection, perhaps due to greater sorption interactions with the aromatic rings present in the polymer backbone. Dual dependence on both size and aromatic interaction was supported by a linear correlation to a combination of aromaticity (sorption) and molecular weight (diffusion) factors, but to neither factor alone (Fig. S22). When compared to Puramem® 280, a commercial polyimide membrane, **SBAD-1** showed higher rejections, although this was accompanied by lower permeances as shown in Table S4 at 22 °C. As the thin film thicknesses were not controlled in this work, the differences in permeance cannot be directly compared because the **SBAD-1** films are considerably thicker.
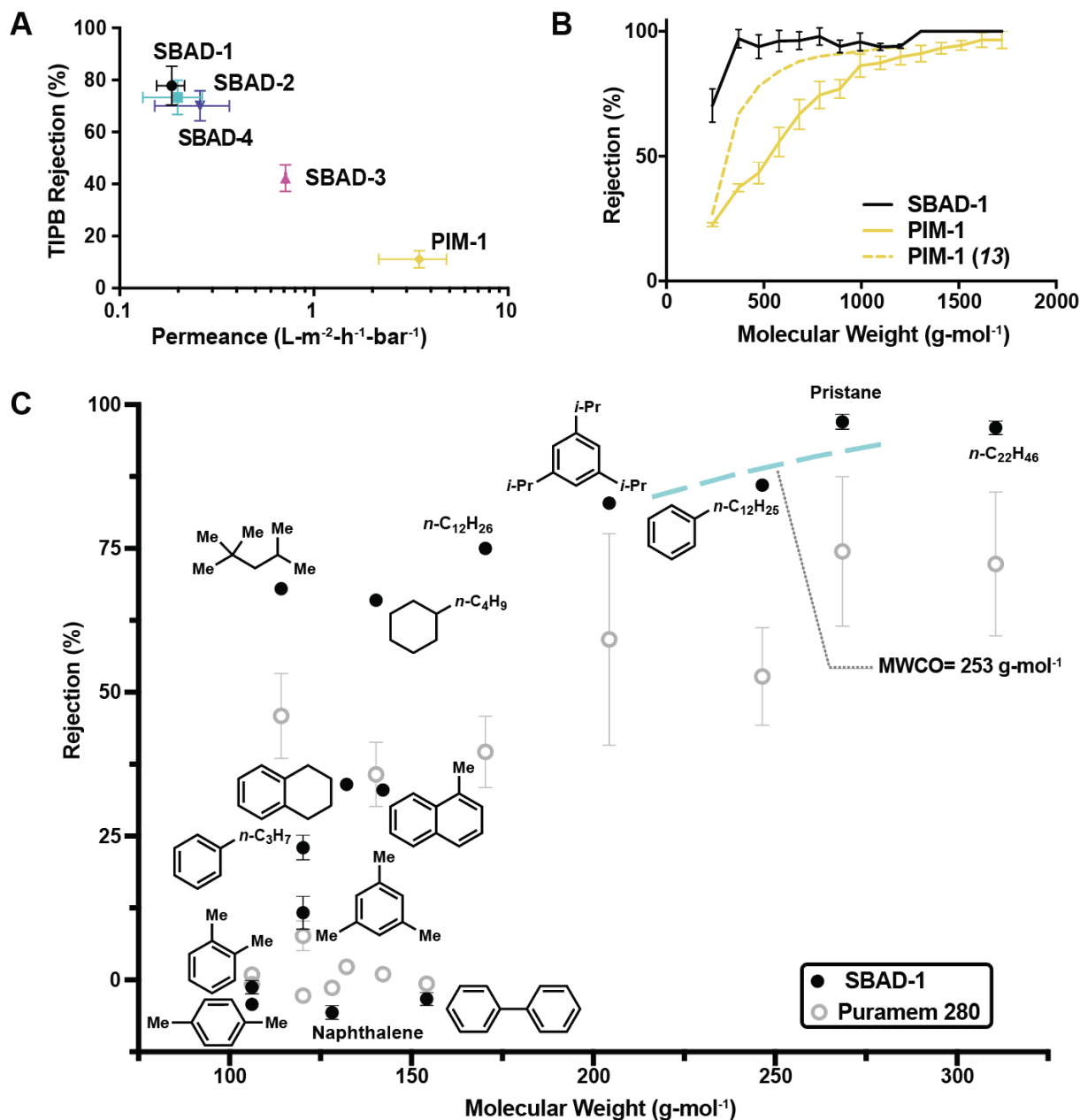
Fig. 2. Dilute hydrocarbon separation performance using polymer thin film composites. (A) TIPB rejection vs. toluene permeance for a 1/99 mol% feed of TIPB/toluene (N=3), 22°C, 15 bar. (B) Molecular weight cut-off curves of **SBAD-1** (N=3) at 30 bar (threshold = 335 g-mol^{-1}), **PIM-1** at 5 bar (1220 g-mol^{-1}), and **PIM-1** data reported at 30 bar (786 g-mol^{-1}) (*11*) for polystyrene standards in toluene at 22°C. The high flux in **PIM-1** in our work limited the applied pressure difference to 5 bar in order to maintain < 5% stage cuts. Data reported by Cook et al. at the same conditions as **SBAD-1** was shown for direct comparison. (C) Hydrocarbon molecular weight cut-

off curve (threshold = 253 g-mol^{-1}, Fig. S21) for **SBAD-1** (N=2) and Puramem® 280 (N=3) from solute mixtures listed in Table S4. Data are the mean of N membranes +/- standard deviation.

The naphtha and kerosene fractions of crude oil make up the primary component of gasoline and jet fuel, respectively. These two fractions typically contain a range of alkanes, alkyl aromatics, and polyaromatics with boiling points from 90°C to 300°C, representing a good candidate for membrane-based hydrocarbon fractionation. A thin-film composite membrane sheet of **SBAD-1** was produced through roll-to-roll coating of the polymer onto a prefabricated Ultem® support (Fig. S23A and B). Membrane coupons from the sheet (diameter 47 mm) were subjected to a complex feed of hydrocarbons that serve as a model naphtha-kerosene fraction. Several large spiral wound modules (Fig. S23C) (containing 1.8 m x 0.2 m of membrane) were also fabricated from the sheet to highlight the scalability of these materials.

Fig. 3A shows the membrane performance (feed composition shown in Table S5) as the ratio of permeate to retentate concentrations plotted against the molecular weights of the components. A permeance of 0.022 ± 0.013 L-m^{-2}-h^{-1}-bar^{-1} for the coupon and 0.076 ± 0.003 L-m^{-2}-h^{-1}-bar^{-1} for the module (Fig. S24) was obtained. This permeance is lower than the dilute mixture experiment (Fig. 2) due to the high osmotic pressure of the complex, multicomponent mixture. However, good separation of molecules of different molecular weights, independent of molecular class, as well as for molecules from different classes without a molecular weight advantage was obtained. Additionally, exposure to temperatures up to 75 °C did not negatively affect membrane performance (Fig. S25). Some notable separation factors (based on coupon data) are shown in Table S6, illustrating the potential of **SBAD-1** for membrane-based concentration of solutes of both low molecular weights and high aromaticity. The values highlighted are comparable with separation factors obtained for liquid xylene isomers using carbon molecular sieve membranes (*19*). Aromatic-rich permeates streams (observed in this work) are useful for the production of plastics and provide a rich source of industrial organic solvents. Fractionation of crude oil into groups of smaller and larger molecules also has direct value in generating products classified by the number of carbons present such as gasoline (C5-12 alkanes and cycloalkanes) and jet fuel (C10-18 alkanes and aromatics). The retentate stream shown in Fig. 3A contains both of these.

SBAD-1 was also challenged with a light shale crude oil to illustrate the potential of membrane materials as an alternative for the fractionation of crude oil. Fig. 3B shows the boiling point distribution of molecules in the feed, permeate and retentate. Approximately 38% of the mixture boiled below 200°C in the feed tested in this work. After passing through a thin film composite of **SBAD-1** the permeate was found to be significantly enriched in the lighter molecules present in the feed, such that more than 60% of the permeate boiled below 200°C. Fig. 3C shows a picture of the crude oil and the lighter colored permeate indicating removal of color bodies that are typically high in molecular weight. Fig. 3D visualizes the differences in GCxGC-FID chromatograms of the feed and permeate, with the three axes representing boiling point (time scale in minutes), polarity (time scale in seconds), and response factor (z-axis). The GCxGC-FID data indicates enrichment of molecules lighter than carbon numbers of 12 or around molecular weight of 170 Da (Fig. 3E). The membrane permeance is low (0.016 L-m^{-2}-h^{-1}-bar^{-1}) as the thin film fabrication process has not yet been optimized to create more productive composites. Overall, the **SBAD-1** membrane-based separation demonstrated selectivity for low molecular weight saturated molecules in the naphtha and early kerosene boiling range with slight permeation of higher molecular weight linear paraffins.
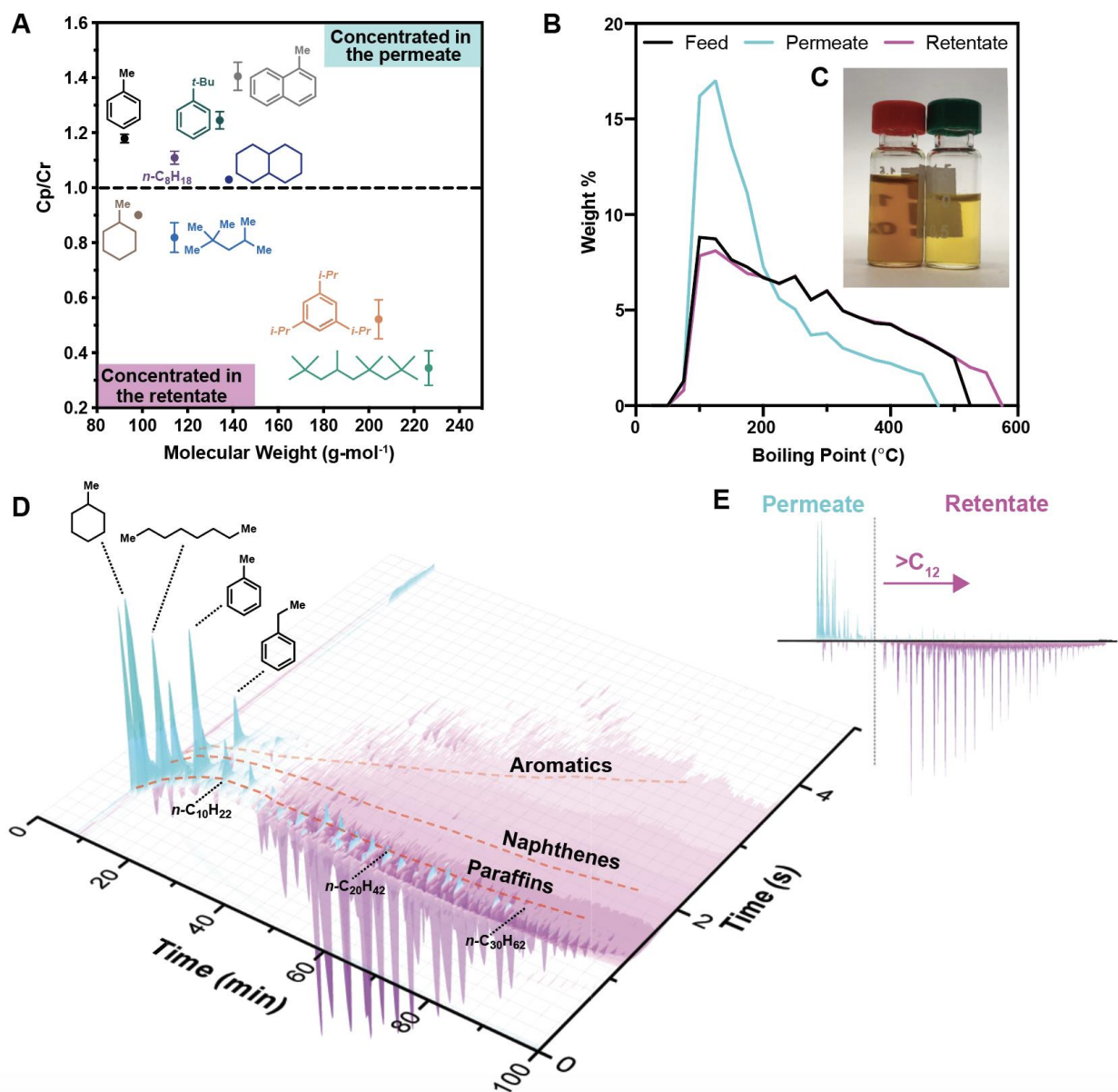
Fig. 3. Synthetic and real crude oil separation performance using SBAD-1 thin film composites. (A) Ratio of concentrations in permeate vs. retentate of components in a complex, model crude oil fractionated by a thin film composite membrane coupon of **SBAD-1** (*N*=3); 40 bar 22°C. Molecules above the reference line were more concentrated in the permeate compared to the feed while the molecules below were more concentrated in the retentate. Data are the mean of 3 membranes +/- standard deviation. (B) Boiling point distribution of feed, permeate and retentate from **SBAD-1** membrane fractionation of shale-based crude oil. (C) Picture of feed (left) and permeate (right) from **SBAD-1** membrane fractionation of real shale-based light whole crude oil. (D) GCxGC-FID analysis of membrane fractionation of shale-based crude oil at 130°C and 55 bar showing the feed chromatogram subtracted from the permeate chromatogram. Teal elution peaks are concentrated in the permeate, whereas the magenta elution peaks are concentrated in the membrane retentate. General hydrocarbon classifications are highlighted with dashed red lines to guide the eye. (E) Side view of GCxGC-FID (shown in D) showing the carbon number partition of real crude oil obtained by **SBAD-1**.

This result is similar to a boiling point separation of a complex hydrocarbon mixture, but without expending the energy associated with vaporization. A clear "inter-class" separation of the crude was observed with a preferential order of permeation: naphthenes, linear paraffins, aromatics, and branched paraffins (Fig. S26 and Table S7). Moreover, "intra-class" size-based separation also occurred for each of these individual classes of hydrocarbons, such that the permeate was enriched in the low boiling (or "light") compounds in the crude oil (Fig. S27). Although we did not specifically explore fouling effects from the real crude feed, the permeance and separation factors changed minimally over a period of two months during synthetic crude testing at temperatures ranging from 25 °C to 75 °C (Fig. S25).

An interesting distinction emerges when comparing traditional binary separation experiments (i.e., toluene/TIPB) and dilute multicomponent hydrocarbon separations with the complex mixture fractionation experiments (i.e., fractionation of lab-made and real crude oil). While molecular weight cut-off and rejection are important figures of merit for dilute separations such as water purification and nanofiltration, the utility of this metric is less clear in the case of complex mixture fractionation where there is no discrete solvent or solute: every molecule in crude oil is a solvent. In this case, each molecule in the mixture experiences highly nonideal coupling effects (e.g., diffusion and sorption) during permeation. Moreover, the osmotic effects in this crude oil system are complex and certainly contribute towards reducing the fluxes relative to the diluted mixtures shown in Fig. 2. The membrane-based crude oil separation occurs via a combination of diffusion-based selection processes as well as solvent-membrane (and solvent-solvent) interactions, which further reinforces the importance of testing real mixtures. Beyond testing industrial feeds, it will be important to establish how these materials fit into an energy-efficient membrane fractionation process (*20*). To produce distillation-like products through membrane fractionation, a cascade of membrane materials such as **SBAD-1**, capable of fractionating feeds across a specific range of hydrocarbon sizes, will be necessary (Fig. S28).

The results described here highlight that the dibenzodioxin connection between spirocyclic monomers that characterizes **PIM-1**-like materials is not necessary to enable meaningful small-molecule membrane-based separations. We speculate that the advantageous properties of SBAD-based membranes derive from the nature of the aromatic nitrogen-carbon linkage, which has long been known to demonstrate hindered rotation (*21*). This connection between spirocyclic and aromatic building blocks gives rise to bulk rigidity and low swelling, isolated and large micropores, and enough segmental mobility to allow migration of molecules between micropores at rates influenced by both molecular size and molecular type.

Together, these properties make the SBAD family promising for the separation of small-sized molecules spanning the organic solvent reverse osmosis and the lower end of the organic solvent nanofiltration range (100-350 g-mol^{-1}) in complex mixtures such as crude oil. Most other membranes that operate in similar regimes require post-polymerization or post-fabrication modifications (e.g., crosslinking) that can be costly and difficult to scale up. In contrast, the polymers used here can be tailored with simple changes in composition and performance. The proposed dependence of SBAD performance on both pore structure and dynamic motion enables complex mixture fractionation that may be scalable and translatable to real crude oil fractions.

References and Notes:

1. International Energy Agency, "World Balance IEA Sankey Diagram". (2017).

2. National Academies of Sciences Engineering and Medicine, *A Research Agenda for Transforming Separation Science.* (The National Academies Press, Washington, DC, 2019).

3. R. P. Lively, D. S. Sholl, From water to organics in membrane separations. *Nat. Mater.* **16**, 276-279 (2017).

4. N. B. McKeown, P. M. Budd, Polymers of intrinsic microporosity (PIMs): organic materials for membrane separations, heterogeneous catalysis and hydrogen storage. *Chem. Soc. Rev.* **35**, 675-683 (2006).

5. W. J. Koros, C. Zhang, Materials for next-generation molecularly selective synthetic membranes. *Nat. Mater.* **16**, 289-297 (2017).

6. C. G. Bezzu et al., A Spirobifluorene-Based Polymer of Intrinsic Microporosity with Improved Performance for Gas Separation. *Adv. Mater.* **24**, 5930-5933 (2012).

7. R. Swaidan, B. S. Ghanem, E. Litwiller, I. Pinnau, Pure- and mixed-gas CO_2/CH_4 separation properties of PIM-1 and an amidoxime-functionalized PIM-1. *J. Membr. Sci.* **457**, 95-102 (2014).

8. M. Cook, P. R. J. Gaffney, L. G. Peeva, A. G. Livingston, Roll-to-roll dip coating of three different PIMs for Organic Solvent Nanofiltration. *J. Membr. Sci.* **558**, 52-63 (2018).

9. P. Marchetti, M. F. J. Solomon, G. Szekely, A. G. Livingston, Molecular Separation with Organic Solvent Nanofiltration: A Critical Review. *Chem. Rev.* **114**, 10735-10806 (2014).

10. D. Fritsch, P. Merten, K. Heinrich, M. Lazar, M. Priske, High performance organic solvent nanofiltration membranes: Development and thorough testing of thin film composite membranes made of polymers of intrinsic microporosity (PIMs). *J. Membr. Sci.* **401**, 222-231 (2012).

11. P. Ruiz-Castillo, S. L. Buchwald, Applications of palladium-catalyzed C–N cross-coupling reactions. *Chem. Rev.* **116**, 12564-12649 (2016).

12. N. C. Bruno, N. Niljianskul, S. L. Buchwald, N-Substituted 2-Aminobiphenylpalladium Methanesulfonate Precatalysts and Their Use in C–C and C–N Cross-Couplings. *J. Org. Chem.* **79**, 4161-4166 (2014).

13. Foster, A. B et al., Understanding the Topology of the Polymer of Intrinsic Microporosity PIM-1: Cyclics, Tadpoles, and Network Structures and Their Impact on Membrane Performance. *Macromolecules*. **53**, 569-583 (2020).

14. M. Heuchel, D. Fritsch, P. M. Budd, N. B. McKeown, D. Hofmann, Atomistic packing model and free volume distribution of a polymer with intrinsic microporosity (PIM-1). *J. Membr. Sci.* **318**, 84-99 (2008).

15. L. J. Abbott, K. E. Hart, C. M. Colina, Polymatic: a generalized simulated polymerization algorithm for amorphous polymers. *Theor. Chem. Acc.* **132** (2013).

16. T. F. Willems, C. Rycroft, M. Kazi, J. C. Meza, M. Haranczyk, Algorithms and tools for high-throughput geometry-based analysis of crystalline porous materials. *Microporous Mesoporous Mater.* **149**, 134-141 (2012).

17. C. Nagel et al., Free volume distributions in glassy polymer membranes: Comparison between molecular modeling and experiments. *Macromolecules* **33**, 2242-2248 (2000).

18. J. L. Duda, I. H. Romdhane, R. P. Danner, Diffusion in Glassy-Polymers - Relaxation and Antiplasticization. *J. Non-Cryst. Solids* **172**, 715-720 (1994).

19. D. Y. Koh, B. A. McCool, H. W. Deckman, R. P. Lively, Reverse osmosis molecular differentiation of organic liquids using carbon molecular sieve membranes. *Science* **353**, 804-807 (2016).

20. B.A. McCool, D.A. Bhandari, Y.V. Joshi, US Patent App No. 20190367820A1, (2019).

21. A. Mannschreck, H. Muensch, Internal rotation about the N-aryl bond in ortho-disubstituted anilines and anilinium ions. *Tetrahedron Lett.* **9**, 3227-3230 (1968).

22. H. Y. Jang et al., Torlon (R) hollow fiber membranes for organic solvent reverse osmosis separation of complex aromatic hydrocarbon mixtures. *AIChE J.* **65**, e16757 (2019).

23. N. C. Bruno, M. T. Tudge, S. L. Buchwald, Design and Preparation of New Palladium Precatalysts for C-C and C-N Cross-Coupling Reactions. *Chem. Sci.* **4**, 916-920 (2013).

24. L. Hintermann, Expedient syntheses of the N-heterocyclic carbene precursor imidazolium salts IPr·HCl, IMes·HCl and IXy·HCl. Beilstein *J. Org. Chem.* **3**, 22 (2007).

25. X.-X. Zhang, J. P. Sadighi, T. W. Mackewitz, S. L. Buchwald, Efficient synthesis of well-defined, high molecular weight, and processible polyanilines under mild conditions via palladium-catalyzed amination. *J. Am. Chem. Soc.* **122**, 7606-7607 (2000).

26. B.-J. Jung, J.-I. Lee, H. Y. Chu, L.-M. Do, H.-K. Shim, Synthesis of novel fluorene-based poly (iminoarylene) s and their application to buffer layer in organic light-emitting diodes. *Macromolecules* **35**, 2282-2287 (2002).

27. Y. Liao, H. Wang, M. Zhu, A. Thomas, Efficient Supercapacitor Energy Storage Using Conjugated Microporous Polymer Networks Synthesized from Buchwald–Hartwig Coupling. *Adv. Mater.* **30**, 1705710 (2018).

28. Y. Liao, J. Weber, B. M. Mills, Z. Ren, C. F. Faul, Highly efficient and reversible iodine capture in hexaphenylbenzene-based conjugated microporous polymers. *Macromolecules* **49**, 6322-6333 (2016).

29. K. Jiang, L. Zhang, Y. Zhao, J. Lin, M. Chen, Palladium-Catalyzed Cross-Coupling Polymerization: A New Access to Cross-Conjugated Polymers with Modifiable Structure and Tunable Optical/Conductive Properties. *Macromolecules* **51**, 9662-9668 (2018).

30. B. P. Fors, D. A. Watson, M. R. Biscoe, S. L. Buchwald, A Highly Active Catalyst for Pd-Catalyzed Amination Reactions: Cross-Coupling Reactions Using Aryl Mesylates and the Highly Selective Monoarylation of Primary Amines Using Aryl Chlorides. *J. Am. Chem. Soc.* **130**, 13552-13554 (2008).

31. T. A. Barbari, W. J. Koros, D. R. Paul, Gas-Transport in Polymers Based on Bisphenol-A. *J. Polym. Sci. B Polym. Phys.* **26**, 709-727 (1988).

32. M. R. Kosuri, W. J. Koros, Defect-free asymmetric hollow fiber membranes from Torlon®, a polyamide–imide polymer, for high-pressure CO2 separations. *J. Membr. Sci.* **320**, 65-72 (2008).

33. M. F. Jimenez-Solomon, Q. Song, K. E. Jelfs, M. Munoz-Ibanez, A. G. Livingston, Polymer nanofilms with enhanced microporosity by interfacial polymerization. *Nat. Mater.* **15**, 760-767 (2016).

34. H. Sun, Force field for computation of conformational energies, structures, and vibrational frequencies of aromatic polyesters. *J. Comput. Chem.* **15**, 752-768 (1994).

35. M. Frisch et al., Gaussian 16. Revision A 3. (2016).

36. S. Plimpton, Fast Parallel Algorithms for Short-Range Molecular Dynamics. *J. Comput. Phys.* **117**, 1-19 (1995).

37. T. F. Willems, C. H. Rycroft, M. Kazi, J. C. Meza, M. Haranczyk, Algorithms and tools for high-throughput geometry-based analysis of crystalline porous materials. *Microporous Mesoporous Mater.* **149**, 134-141 (2012).

38. M. Pinheiro, R. L. Martin, C. H. Rycroft, M. Haranczyk, High accuracy geometric analysis of crystalline porous materials. *CrystEngComm* **15**, 7531-7538 (2013).

39. L. M. Robeson, Correlation of separation factor versus permeability for polymeric membranes. *J. Membr. Sci.* **62**, 165-185 (1991).

40. K. E. Hart, J. M. Springmeier, N. B. McKeown, C. M. Colina, Simulated swelling during low-temperature N_2 adsorption in polymers of intrinsic microporosity. *Phys. Chem. Chem. Phys.* **15**, 20161-20169 (2013).

Acknowledgments

J.R.J. GCxGC analysis was conducted by S.J.H. Complex mixture separation results were confirmed by R.M., D.K., J.K., N.R. and J.R.J at separate facilities. Temperature resistance of membranes was investigated by N.R. and J.R.J. B.A.M., A.G.L., R.P.L., and M.G.F. conceived the research. **Competing interests:** A.G.L. serves as a non-Executive Director of Evonik Membrane Extraction Technology UK Limited. **Data and materials availability:** Detailed descriptions of materials and methods, monomer synthesis, polymer synthesis, polymer model generation and analysis, powder characterization, membrane fabrication, spectroscopic characterization, and separation performance are in the supplementary materials. K.A.T., R.M., B.A.M., R.P.L., M.G.F. are inventors on patent applications (US20190275469, US20190390126, and, 62/640,253) submitted by Georgia Tech Research Corporation and ExxonMobil Research and Engineering that covers SBAD polymers, membrane fabrications and crude oil fractionation applications. All data needed to evaluate the conclusions in the paper are present in the paper or the Supplementary Materials.

Supplementary Materials:

Materials and Methods

Figs. S1-S28

Tables S1-S7

NMR Spectra

References (*23-40*)